A High-Order Sliding Mode Observer for Sensorless Control ofDFIG-Based Wind Turbines

Mohamed Benbouzid, Brice Beltran, Hervé Mangel, Abdeslam Mamoune

A High-Order Sliding Mode Observer for Sensorless Control of DFIG-Based Wind Turbines

Mohamed Benbouzid, Brice Beltran, Hervé Mangel and Abdeslam Mamoune

***Abstract*—This paper deals with the sensorless control of a doubly-fed induction generator (DFIG) based wind turbine. The sensorless control scheme is based on a high-order sliding mode (HOSM) observer to estimate the DFIG rotational speed. Indeed, high-order sliding mode observers provide theoretically finite time exact state observation and estimation of absolutely continuous unknown inputs. The proposed global control strategy combines an MPPT using a high-order sliding mode speed observer and a high-order sliding mode for the DFIG control. This strategy presents attractive features such as chattering-free behavior, finite reaching time, robustness and unmodeled dynamics (generator and turbine).**

Simulations using the wind turbine simulator FAST on a 1.5-MW three-blade wind turbine are carried out for the validation of the proposed sensorless control strategy.

***Index Terms*—Wind turbine, doubly-fed induction generator, sensorless control, observer, high-order sliding mode.**

NOMENCLATURE

v	=	Wind speed;
ρ	=	Air density;
R	=	Rotor radius (m);
P_a	=	Aerodynamic power;
T_a	=	Aerodynamic torque;
λ	=	Tip speed ratio;
C_p	=	Power coefficient;
ω_{mr}	=	Wind turbine speed;
T_g	=	Generator electromagnetic torque;
J_t	=	Turbine total inertia;
K_t	=	Turbine total external damping;
s (r)	=	Stator (rotor) index;
d (q)	=	Synchronous reference frame index;
V (I)	=	Voltage (current);
ϕ	=	Flux;
T_{em}	=	Electromagnetic torque;
R	=	Resistance;
L (M)	=	Inductance (mutual inductance);
σ	=	Leakage coefficient, $\sigma = 1 - M^2/L_sL_r$;
ω_r (ω_s)	=	Angular speed (synchronous speed);
s	=	Slip;
p	=	Pole pair number.

M.E.H. Benbouzid, B. Beltran, H. Mangel and A. Mamoune are with the University of Brest, EA 4325 LBMS, Rue de Kergoat, CS 93837, 29238 Brest Cedex 03, France (e-mail: Mohamed.Benbouzid@univ-brest.fr).

I. INTRODUCTION

DFIGs are widely used for variable speed generation and are among the most important generators for wind energy applications (Fig. 1) [1-2]. Indeed, this topology has about 50% fraction of the wind energy market. In this context, their sensorless control has received increasing interest as shaft sensors have drawbacks in terms of maintenance, cost, robustness, and cabling between the sensor and the controller [3-6]. A brief review of the main available sensorless control strategies shows that the proposed speed estimation schemes are quiet sensitive to the generator parameters [4].

In this context, this paper proposes the use of a high-order sliding mode observer for the speed estimation [7-8]. Indeed, compared to other observer, sliding mode has attractive advantages of robustness to disturbances and low sensitivity to the generator parameter variations. Moreover, HOSM will eliminate the chattering phenomenon by using continuous signals instead of switching signals [9-10].

Specifically, the proposed global control strategy combines an MPPT using a HOSM observer and a HOSM for the DFIG control. This strategy presents attractive features such as chattering-free behavior, finite reaching time, robustness and unmodeled dynamics (generator and turbine).

II. DFIG-BASED WIND TURBINE MODELING

The wind turbine modeling is inspired from [10].

A. The Turbine Model

The aerodynamic power captured by the wind turbine is given by

$$P_a = \frac{1}{2}\pi\rho R^2 C_p(\lambda) v^3 \qquad (1)$$

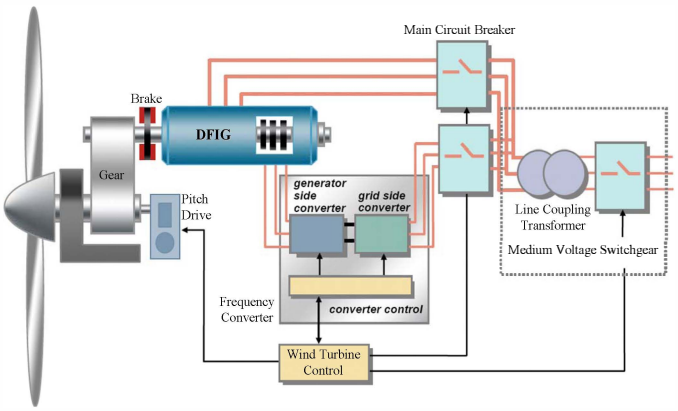

Fig. 1. Schematic diagram of a DFIG-based wind turbine.

where $\lambda = \dfrac{R\omega_{mr}}{v}$ (2)

The rotor power (aerodynamic power) is also defined by

$$P_a = \omega_{mr} T_a \tag{3}$$

The following simplified model is adopted for the turbine (drive train) for control purposes.

$$J_t \dot{\omega}_{mr} = T_a - K_t \omega_{mr} - T_g \tag{4}$$

B. The DFIG Model

For the proposed control strategy, the generator dynamic model written in a synchronously rotating frame *d-q* is given by (5).

$$\begin{cases} V_{sd} = R_s I_{sd} + \dfrac{d\phi_{sd}}{dt} - \omega_s \phi_{sq} \\ V_{sq} = R_s I_{sq} + \dfrac{d\phi_{sq}}{dt} + \omega_s \phi_{sd} \\ V_{rd} = R_r I_{rd} + \dfrac{d\phi_{rd}}{dt} - \omega_r \phi_{rq} \\ V_{rq} = R_r I_{rq} + \dfrac{d\phi_{rq}}{dt} + \omega_r \phi_{rd} \\ \phi_{sd} = L_s I_{sd} + M I_{rd} \\ \phi_{sq} = L_s I_{sq} + M I_{rq} \\ \phi_{rd} = L_r I_{rd} + M I_{sd} \\ \phi_{rq} = L_r I_{rq} + M I_{sq} \\ T_{em} = pM\left(I_{rd} I_{sq} - I_{rq} I_{sd}\right) \end{cases} \tag{5}$$

III. The HOSM Speed Observer

Figure 2 illustrates the main reference frames on which is based the proposed speed observer development.

In this case, θ_s can be easily determined using stator voltage measurements and a PLL.

If the stator flux is assumed to be aligned with the *d*-axis,

$$\begin{cases} \phi_{sd} = \phi_s \\ \phi_{sq} = 0 \end{cases} \tag{6}$$

then, the *d-q* rotor current can be estimated as

$$\begin{cases} \hat{I}_{rd} = \dfrac{\phi_s}{M} - \dfrac{L_s}{M} I_{sd} \\ \hat{I}_{rq} = -\dfrac{L_s}{M} I_{sq} \end{cases}$$

Let us now define θ_r such as

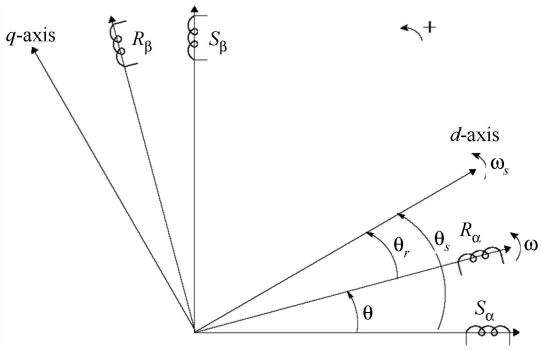

Fig. 2. Stator S_α_S_β, rotor R_α_R_β, and *d-q* reference frames.

$$\hat{I}_{rq} = \sqrt{\frac{2}{3}} \begin{pmatrix} -I_{ra}\sin\theta_r + \dfrac{1}{2} I_{rb}\sin\theta_r \\ + \dfrac{\sqrt{3}}{2} I_{rb}\cos\theta_r + \dfrac{1}{2} I_{rc}\sin\theta_r \\ - \dfrac{\sqrt{3}}{2} I_{rc}\cos\theta_r \end{pmatrix} \tag{7}$$

Using $x = \tan\left(\dfrac{\theta_r}{2}\right)$, I_{rq} can be rewritten as

$$\hat{I}_{rq} = \sqrt{\frac{2}{3}} \begin{pmatrix} -I_{ra}\dfrac{2x}{1+x^2} + \dfrac{1}{2} I_{rb}\dfrac{2x}{1+x^2} \\ + \dfrac{\sqrt{3}}{2} I_{rb}\dfrac{1-x^2}{1+x^2} + \dfrac{1}{2} I_{rc}\dfrac{2x}{1+x^2} \\ - \dfrac{\sqrt{3}}{2} I_{rc}\dfrac{1-x^2}{1+x^2} \end{pmatrix} \tag{8}$$

After some algebraic manipulations, it comes that

$$\hat{I}_{rq} = \frac{1}{1+x^2}\sqrt{\frac{2}{3}} \begin{bmatrix} x^2\left(\dfrac{\sqrt{3}}{2} I_{rc} - \dfrac{\sqrt{3}}{2} I_{rb}\right) \\ + x\left(-2I_{ra} + I_{rb} + I_{rc}\right) \\ + \left(-\dfrac{\sqrt{3}}{2} I_{rc} + \dfrac{\sqrt{3}}{2} I_{rb}\right) \end{bmatrix} \tag{9}$$

This equation can further be rewritten in a compact form

$$\hat{I}_{rq} = \frac{x^2 a + xb + c}{1+x^2} \tag{10}$$

$$at^2 + bt + c = 0 \quad \text{with} \begin{cases} a = \sqrt{\dfrac{3}{2}}\hat{I}_{rq} + \dfrac{\sqrt{3}}{2}\left(I_{rb} - I_{rc}\right) \\ b = 2I_{ra} - I_{rc} - I_{rc} \\ c = \sqrt{\dfrac{3}{2}}\hat{I}_{rq} - \dfrac{\sqrt{3}}{2}\left(I_{rb} - I_{rc}\right) \end{cases}$$

The solutions of this equation are the following.

$$\begin{cases} x_1 = \dfrac{-b+\sqrt{b^2-4ac}}{2a} \\ x_2 = \dfrac{-b-\sqrt{b^2-4ac}}{2a} \end{cases} \tag{11}$$

Now we will estimate the derivative of the following value $z = 2\arctan x_1$ using a second-order sliding mode. The same result is obtained with $\arctan x_2$.

The main problem with high-order sliding mode algorithm implementations is the increased required information. Indeed, the implementation of an n^{th}-order controller requires the knowledge of $\dot{S}$, $\ddot{S}$, $\dddot{S}$,..., $S^{(n-1)}$. The exception is the *supertwisting* algorithm, which only needs information about the sliding surface *S*. Therefore, the proposed speed observer is designed using this algorithm [11].

Let us therefore consider the following observer

$$\begin{cases} \dot{y} = -B_2 \operatorname{sgn}(e) \\ \dot{W} = y - B_1 |e|^{\frac{1}{2}} \operatorname{sgn}(e) \end{cases} \tag{12}$$

where the constants B_1 and B_2 are defined as

$$\begin{cases} B_2 > \phi \\ B_1^{\,2} > \dfrac{4(B_2+\phi)^2}{2(B_2-\phi)} \end{cases} \tag{13}$$

Lets us consider the following tracking error.

$$\begin{cases} e = W - z \\ \dot{e} = y - B_1 |e|^{\frac{1}{2}} \operatorname{sgn}(e) - \dot{z} \\ \ddot{e} = -B_2 \operatorname{sgn}(e) - B_1 \dfrac{\dot{e}}{2|e|^{\frac{1}{2}}} - \ddot{z} \end{cases} \tag{14}$$

Assume now, for simplicity, that the initial values are $e = 0$ and $\dot{e} = \dot{e}_0 > 0$ at $t = 0$. Let e_M be the intersection of the curve $\ddot{e} = -(B_2 - \phi)$ with $\dot{e} = 0$, $|\ddot{z}| < \phi$. We have then

$$2e_M (B_2 - \phi) = \dot{e}_0^2 \tag{15}$$

$$e > 0, \dot{e} < -(B_2+\phi)\frac{2e_M^{1/2}}{B_1} \Rightarrow \ddot{e} > 0$$

Thus, the majorant curve with $e > 0$ may be taken as

$$\begin{cases} \dot{e}_0^{\,2} = 2(B_2 - \phi)(e_M - e) \quad \text{with } \dot{e} > 0 \\ e = e_M \quad \text{with } 0 \geq \dot{e} > -(B_2+\phi)\dfrac{2e^{\frac{1}{2}}}{B_1} \\ \dot{e} = \dot{e}_M = -(B_2+\phi)\dfrac{2e_M^{\frac{1}{2}}}{B_1} \quad \text{with } \dot{e} < -(B_2+\phi)\dfrac{2e^{\frac{1}{2}}}{B_1} \end{cases} \tag{16}$$

Let the trajectory next intersection with $e = 0$ axis be e_1. Then, obviously

$$|\dot{e}_1 / \dot{e}_0| \leq q \quad \text{with } q = |\dot{e}_M / \dot{e}_0| = \sqrt{\frac{\left(\frac{2}{B_1}\right)^2 (B_2+\phi)^2}{2(B_2-\phi)}} \tag{17}$$

Extending the trajectory into the half plane $e < 0$ and carrying-out a similar reasoning show that successive crossings of the $e = 0$ axis satisfy the inequality

$$\left|\frac{\dot{e}_{i+1}}{\dot{e}_i}\right| \leq q$$

The $q < 1$ condition is sufficient for the algorithm convergence. Indeed, the real trajectory consists of an infinite number of segments. The total variance is given by

$$Var(\dot{e}) = \sum |\dot{e}_i| \leq |\dot{e}_0|\left(1 + q + q^2 + \ldots\right) = \frac{|\dot{e}_0|}{1-q} \tag{18}$$

Therefore, the algorithm obviously converges.

The convergence time is to be estimated now. Consider an auxiliary variable

$$\eta = y - \dot{z} \tag{19}$$

$\eta = \dot{e}$ when $e = 0$. Thus, η tends to zero. Its derivative

$$\ddot{e} = -B_2 \operatorname{sgn}(e) - G \tag{20}$$

satisfies the inequalities

$$0 < B_2 - \phi \leq -\dot{\eta}\operatorname{sgn}(e_{I_{rd}}) \leq B_2 + \phi \tag{21}$$

The real trajectory consists of an infinite number of segments between $\eta_i = \dot{e}_i$ and $\eta_{i+1} = \dot{e}_{i+1}$ associated to the time t_i and t_{i+1}, respectively. Consider t_c, the total convergence time.

$$\begin{cases} t_c = \sum (t_{i+1} - t_i) \le \sum \dfrac{|\eta_i|}{B_2 - \phi} \\ t_c \le \dfrac{1}{B_2 - \phi} \sum |\dot{e}_i| \\ t_c \le \dfrac{|\dot{e}_0|}{(B_2 - \phi)(1-q)} \end{cases} \quad (22)$$

This means that the observer objective is achieved. It exist t_c such as $\omega_r = \dot{W}$.

IV. HOSM Control of the DFIG-Based Wind Turbine

The above designed HOSM observer is now exploited for the control of a DFIG-based wind turbine. The adopted control strategy is also the HOSM approach developed in [9]. It is summarily presented in this section.

For simplification purposes, the *q*-axis is aligned with the stator voltage and the stator resistance is neglected. These will lead to.

$$\begin{cases} \dfrac{dI_{rd}}{dt} = \dfrac{1}{\sigma L_r}\left(V_{rd} - R_r I_{rd} + s\omega_s \sigma L_r I_{rq} - \dfrac{M}{L_s}\dfrac{d\phi_{sd}}{dt} \right) \\ \dfrac{dI_{rq}}{dt} = \dfrac{1}{\sigma L_r}\left(V_{rq} - R_r I_{rq} - s\omega_s \sigma L_r I_{rd} - s\omega_s \dfrac{M}{L_s}\phi_{sd} \right) \\ T_{em} = -p\dfrac{M}{L_s}\phi_{sd} I_{rq} \end{cases} \quad (23)$$

Setting the reactive power to zero will therefore lead to the rotor reference current.

$$I_{rd\_ref} = \frac{V_s}{\omega_s M} \quad (24)$$

The control objective is to optimize the wind energy capture by tracking the optimal torque T_{ref}. This objective can be formulated by the following tracking errors.

$$\begin{cases} e_{I_{rd}} = I_{rd} - I_{rd\_ref} \\ e_{T_{em}} = T_{em} - T_{ref} \end{cases} \quad (25)$$

In short, the following second-order sliding mode controller based on the supertwisting algorithm is therefore adopted [9].

$$\begin{cases} V_{rd} = y_1 - B_1 \left| e_{I_{rd}} \right|^{\frac{1}{2}} \operatorname{sgn}\left(e_{I_{rd}} \right), \dot{y}_1 = -B_2 \operatorname{sgn}\left(e_{I_{rd}} \right) \\ V_{rq} = y_2 + B_3 \left| e_{T_{em}} \right|^{\frac{1}{2}} \operatorname{sgn}\left(e_{T_{em}} \right), \dot{y}_2 = +B_4 \operatorname{sgn}\left(e_{T_{em}} \right) \end{cases} \quad (26)$$

where the constants B_1, B_2, B_3, and B_4 are defined as

$$\begin{cases} B_1^2 > \dfrac{2\sigma^2 L_r^2 \left(\dfrac{B_2}{\sigma L_r} + \Phi_1 \right)}{\left(\dfrac{B_2}{\sigma L_r} - \Phi_1 \right)}, B_2 > \sigma L_r \Phi_1, \left| \dot{G}_1 \right| < \Phi_1 \\ B_3^2 > 2\left(\dfrac{\sigma L_s L_r}{pM} \right)^2 \dfrac{\left(p\dfrac{M}{\sigma L_s L_r} B_4 + \Phi_2 \right)}{\left(p\dfrac{M}{\sigma L_s L_r} B_4 - \Phi_2 \right)}, B_4 > \dfrac{\sigma L_s L_r}{pM}\Phi_2 \\ \left| \dot{G}_2 \right| < \Phi_2 \end{cases} \quad (27)$$

The above proposed sensorless HOSM control strategy using a HOSM speed observer is illustrated by the block diagram in Fig. 3.

V. FAST Code-Based Simulations Results

The proposed HOSM sensorless control strategy has been tested for validation using the NREL FAST code [12].

An interface has been developed between FAST and Matlab-Simulink® to implement the proposed HOSM observer and control strategy in Simulink convenient block diagram form (Fig. 4).

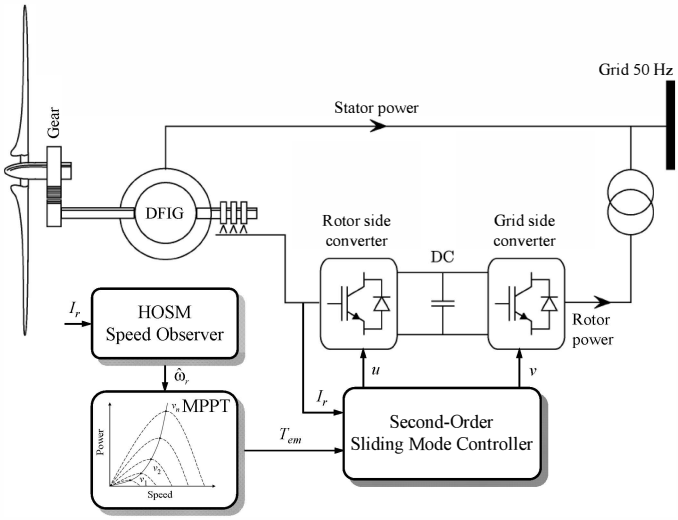

Fig. 3. The proposed sensorless control structure.

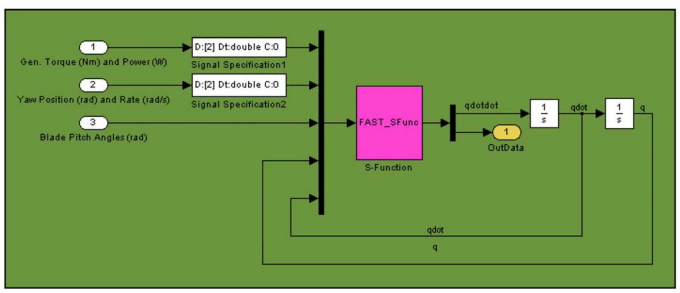

Fig. 4. FAST wind turbine block.

Numerical validations, using FAST with Matlab-Simulink® have been carried out on the NREL WP 1.5-MW wind turbine. The validation tests were performed using turbulent FAST wind data shown by Fig. 5.

The performances of the proposed HOSM speed observer are illustrated by Fig. 6. The achieved results show quiet good tracking chattering free performances.

Figures 7 and 8 illustrate the HOSM sensorless control performances in terms of DFIG rotor current and wind turbine torque. In this case quiet good tracking performances are achieved according to the wind fluctuations. As is [9], the sensorless control strategy does not induce mechanical stress as there is no chattering in the wind turbine torque (Fig. 8).

VI. Conclusion

This paper dealt with a sensorless control scheme of a DFIG-based wind turbine.

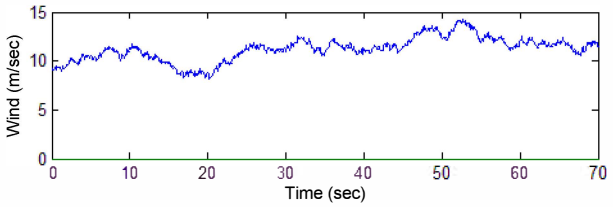

Fig. 5. Wind speed profile.

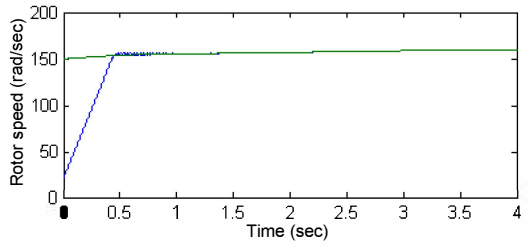

Fig. 6. Rotor speed: Observer (blue) and real (green).

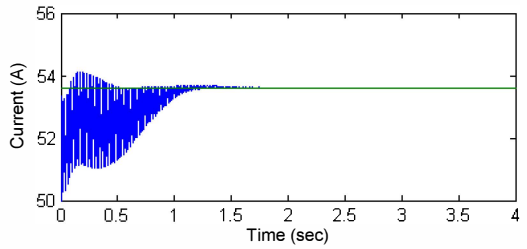

Fig. 7. Current I_{rd} tracking performance: Reference (green) and real (blue).

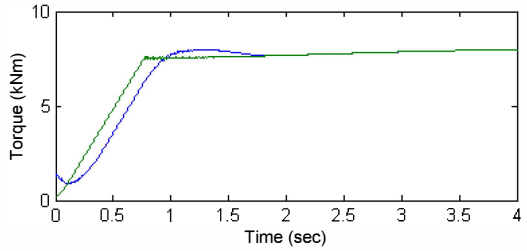

Fig. 8. Torque tracking performance: Reference (green) and real (blue).

The proposed sensorless control approach was based on a high-order sliding mode observer to estimate the DFIG speed. Specifically, the proposed global control strategy combines an MPPT using a HOSM observer and a HOSM for the DFIG control.

Simulations using the wind turbine simulator FAST on a 1.5-MW three-blade wind turbine have led to very promising results that show the effectiveness of the proposed HOSM sensorless control scheme.

Appendix

Characteristics of the Simulated Wind Turbine

Number of blades	3
Rotor diameter	70 m
Hub height	84.3 m
Rated power	1.5 MW
Turbine total inertia	4.4532×10^5 kg m^2

Parameters of the Simulated DFIG

$R_s = 0.005\ \Omega$, $L_s = 0.407$ mH, $R_r = 0.0089\ \Omega$, $L_r = 0.299$ mH
$M = 0.016$ mH, $p = 2$

References

[1] M. Liserre, R. Cardenas, M. Molinas and J. Rodriguez, "Overview of multi-MW wind turbines and wind parks," *IEEE Trans. Industrial Electronics*, vol. 58, n°4, pp. 1081-1095, April 2011.

[2] M. Tazil, V. Kumar, R.C. Bansal, S. Kong, Z.Y. Dong, W. Freitas and H.D. Mathur, "Three-phase doubly fed induction generators: an overview," *IET Power Applications*, vol. 4, n°2, pp. 75-89, February 2010.

[3] M. Pucci and M. Cirrincione, "Neural MPPT control of wind Generators with induction machines without speed sensors," *IEEE Trans. Industrial Electronics*, vol. 58, n°1, pp. 37-47, January 2011.

[4] S. Yang and V. Ajjarapu, "A speed-adaptive reduced-order observer for sensorless vector control of doubly fed induction generator-based variable-speed wind turbines," *IEEE Trans. Energy Conversion*, vol. 25, n°3, pp. 891-900, September 2010.

[5] R. Cardenas, R. Pena, P. Wheeler, J. Clare, G. Asher and J. Proboste, "MRAS observers for sensorless control of doubly-fed induction generators," *IEEE Trans. Power Electronics*, vol. 23, n°3, pp. 1075-1084, May 2008.

[6] R. Pena, R. Cardenas, J. Proboste, G. Asher and J. Clare, "Sensorless control of doubly-fed induction generators using a rotor-current-based MRAS observer," *IEEE Trans. Industrial Electronics*, vol. 55, n°53, pp. 330-339, January 2008.

[7] A. Ferreira, F.J. Bejarano and L.M. Fridman, "Robust control with exact uncertainties compensation: With or without chattering?," *IEEE Trans. Control Systems Technology*, vol. 19, n°5, pp. 969-975, September 2011.

[8] Y. Feng, J. Zheng, X. Yu and N.V. Truong, "Hybrid terminal sliding-mode observer design method for a permanent-magnet synchronous motor control system," *IEEE Trans. Industrial Electronics*, vol. 56, n°9, pp. 3424-3431, September 2009.

[9] B. Beltran, M.E.H. Benbouzid and T. Ahmed-Ali, "Second-order sliding mode control of a doubly fed induction generator driven wind turbine," *IEEE Trans. Energy Conversion*, DOI: 10.1109/TEC.2011.2181515, 2012.

[10] B. Beltran, T. Ahmed-Ali and M.E.H. Benbouzid, "High-order sliding mode control of variable speed wind turbines," *IEEE Trans. Industrial Electronics*, vol. 56, n°9, pp. 3314-3321, September 2009.

[11] A. Levant and L. Alelishvili, "Integral high-order sliding modes," *IEEE Trans. Automatic Control*, vol. 52, n°7, pp. 1278-1282, July 2007.

[12] http://wind.nrel.gov/designcodes/simulators/fast/.